Integrative Biology

Accepted Manuscript

ROYAL SOCIETY OF CHEMISTRY

www.rsc.org/ibiology

Integrative Biology

RSCPublishing

ARTICLE

Substrate elasticity modulates the responsiveness of mesenchymal stem cells to commitment cues

Cite this: DOI: 10.1039/x0xx00000x

S. Gobaa,[a,¶] S. Hoehnel[a,¶] and M. P. Lutolf [a,b*]

Received 00th January 2012,
Accepted 00th January 2012

DOI: 10.1039/x0xx00000x

www.rsc.org/

Fate choices of stem cells are regulated in response to a complex array of biochemical and physical signals from their microenvironmental niche. Whereas the molecular composition and the role of mechanical niche cues have been extensively studied, relatively little is known about how both effectors act in concert to modulate stem cell fate. Here we utilized a recently developed artificial niche microarray platform to investigate whether the stiffness of a cell culture substrate influences how niche signaling factors exert their role on adipogenic differentiation of human mesenchymal stem cells (hMSC). We found that substrate stiffness imposes a strictly non-overlapping range of differentiation, highlighting the dominance of physical over the biochemical factors. At a given stiffness, a significant protein-dependent effect on adipogenic differentiation was observed. Furthermore, we show that synergistic interactions between proteins can also be driven by the substrate stiffness. Our results thus highlight the importance of considering the mechanical properties of a target tissue when investigating biochemical niche signals *in vitro*.

Introduction

Cellular niches are composed of numerous biomolecules including growth factors, cell-cell interaction proteins and extracellular matrix (ECM) signals. Apart from these biochemical regulators, various stem cell types have been shown to alter their fate in response to biophysical properties of the niche including its elasticity[1] or topography.[2, 3] For instance, hMSC actively sense the mechanical properties of their environment to differentially commit to osteogenic, myogenic or neuronal lineages depending on the elasticity of their substrates.[4-6] However, to what extent interactions between biophysical and biochemical niche cues modulate stem cell fate remains unclear.[7]

Stem cell niches are complex entities whose effects on stem cell fate are difficult to elucidate directly *in vivo* where the loss of a biomolecule can be readily restored or compensated by other signals in the surrounding.[8] Traditional *in vitro* culture methods are often poorly suited to dissect the complex cocktail of biochemical cues that balance stem cell self-renewal and differentiation. To overcome this limitation, microenvironment arrays have been developed for the screening of extrinsic cell fate regulators via (high-throughput) robotic spotting of biomolecule combinations.[9-12] However, these platforms lack the ability to simultaneously explore biophysical effectors, as they were produced on glass or acrylamide gels with fixed composition. In an effort to enrich the capabilities of such screening platforms by enabling the study of biochemical regulators in the context of variable substrates stiffness, we have developed artificial niche arrays consisting of poly(ethylene glycol) (PEG)-based hydrogel microwell arrays of variable substrate stiffness wherein each microwell can be functionalized independently with a desired combination of biomolecules.[13]

In the present work our aim was to better understand the interplay of biochemical and biophysical factors that control adipogenic differentiation of hMSCs. We therefore chose to simultaneously interrogate the effect of multiple protein combinations across variable substrate stiffness. This approach allowed us to hierarchically classify the importance of each niche cue in inducing differentiation. We demonstrate that substrate stiffness always overrides the effect of biochemical signals. However, within stiffness categories, the action of proteins accounts for a large part of the adipogenic differentiation with protein effects that are either dominant or context-dependent. Our results stress the importance of considering physical microenvironmental parameters when testing the effect of particular biochemical signaling cues on stem cell fate.

Experimental methods

Measurements of substrate stiffness

Hydrogel discs of 1 mm thickness and 50 µl volume were cast between two SigmaCote (Sigma) treated glass slides. Shear moduli (G') of gels, left to swell for 24h prior to measurements, were obtained using a Bohlin Instruments C-VOR rheometer. Swollen hydrogel disks were placed centrically on the bottom plate. The gap size was lowered to 800 µm (compression: 0.2) to avoid gel movement. A linear frequency sweep was carried

out from 0.1 to 10 Hz with 5% shear stress constantly applied to measure G', G'' and the phase angle Θ. As G' values remained constant over the measured frequency range, the average G' was considered as the equilibrium shear modulus of the network.

Artificial niche array preparation

Hydrogel microwell arrays were prepared as previously described.[13] In brief, thin PEG hydrogel films formed by two 10kDa PEG precursors bearing either thiol or vinylsulfone groups (NOF corporation) were cast at the bottom of four-well plates (Nunc). Three distinct levels of stiffness were obtained by mixing the precursors at different mass to volume ratios. Excess TH-groups (1.2mM) as well as maleimide-functionalized Protein A (85μg ml^{-1}) were introduced in the bulk PEG hydrogel to allow for covalent binding with maleimide-functionalized proteins or Fc-tagged proteins respectively. A topologically structured silicone stamp, custom-made by microfabrication, was used to emboss the partially cross-linked hydrogel film and to transfer desired proteins or protein combinations to the bottom of the imprinted microstructures, i.e. microwells. To achieve this, proteins and protein combinations were pre-mixed in a 384-microtiter master plate in a 10μl volume prior to robotic printing using a QArray DNA spotter (Genetix Ltd.). A software interface (QSoft) was programmed to arrange protein combinations on the final array with two randomized designs. Subsequent to printing and embossing, arrays were de-molded, washed with PBS and UV-sterilized. Passivation of the arrays by overnight treatment with a 0.1% (w/v) Pluronic PE6800 (BASF) at 37°C was carried out to minimize non-specific cell attachment to the non-functionalized PEG surface.

Protein screen

Nine proteins were chosen among known MSC signaling cascades; i.e. Wnt-, BMP- and Notch-pathway. Two cell-cell interaction molecules as well as a fibronectin fragment 9-10 (FN III(9-10)) were also included. A combinatorial screen was performed on the single proteins as well as their combinations of two. A full list of arrayed proteins and respective combinations, concentrations and suppliers are given in Supplementary Table S 1. All proteins were provided as recombinant and carrier-free. The initial bioactivity was guaranteed by the manufacturer. Lyophilized proteins were first reconstituted according to supplier instructions at concentrations between 250 to 1000 μg ml^{-1}. Protein candidates not harboring an Fc-tag were modified with a hetero-bifunctional NHS-PEG-maleimide linker (3.5 kDa, JenKem Technology) for covalent binding to excess thiols in the bulk PEG hydrogel. Of note, bioactivity loss after protein PEGylation was tested and found to be minimal (Supplementary Fig. S2) Proteins were prepared as printing solutions composed of the protein or proteins at a final concentration of 50μg ml-1 in PBS or borate buffer (0.1 M, pH8, Sigma-Aldrich), FN III(9-10) at a concentration of 800 μg ml^{-1}; all containing 30% (v/v) glycerol.

Cell culture

Human MSCs (patient 101001) were purchased from Biopredic. Cells were derived from the iliac crest of a 34 year old male donor and phenotypically characterized by FACS for the presence of the surface antigens CD13, CD90, CD73, CD29, CD166, CD105 and for the absence of CD45, CD31 and CD34. MSCs were obtained as passage 1 cells and expanded to passage 3 (p3) in expansion medium containing α-MEM (Gibco) supplemented with 10% fetal calf serum (FCS, Hyclone, batch AUA33984), 2 mM L-glutamine (Sigma), 100 U ml^{-1} penicillin/ streptomycin (Invitrogen) and 1ng ml^{-1} human FGF2 (Peprotech). Expanded hMSCs were stored as aliquots in FCS containing 10% DMSO (Sigma) in liquid nitrogen until use. The adipogenic potential of the p3 cells was verified by culturing hMSCs in adipogenic differentiation medium for 5 to 21 days consisting of low glucose DMEM (Gibco) supplemented with 20% FCS, 0.5 mM IBMX (Sigma), 60 μM indomethacin (Fluka) and 1 μM dexamethasone (Sigma) (data not shown). For array seeding, hMSCs p3 were unfrozen 24h prior to the experiment in expansion medium not containing FGF2. FGF2 was depleted from the expansion medium from this point onwards to avoid interactions with arrayed proteins. Cells were subsequently trypsinized using 0.05% trypsin/EDTA (Invitrogen) and cell density adjusted to 7.5E4 cells per 4 ml seeding volume per array. After 1h incubation, arrays were washed with PBS to remove non-adherent MSCs. Adipogenesis was induces by culturing the cells in the above mentioned differentiation medium for 11 days.

hMSCs were seeded atop the arrays and captured within the microwells through gravitational sedimentation, where they attached in the presence of FNIII9-10. Unbound cells between microwells or in microwells harboring no cell-adhesive protein were washed off the array using PBS. Numbers of captured cells at day 0 (CellD0) were Poisson distributed across the whole array. We previously reported an optimal seeding density of 7.5E4 cells per seeding volume for arrays probing adipogenic differentiation.[13] Resultantly, the majority of the microwells harbor two to four cells per microwell. Also, across the levels of stiffness, no difference in initial cell distributions could be observed.

Following cell capture, microwell arrays were cultured in adipogenic induction medium for a period of 11 days. To examine the effect of different proteins on adipogenic differentiation, proliferation and cell morphology, arrays were fixed at the end of the culture time and stained with Nile Red (lipid vesicles), DAPI (nuclei) or Phalloidin (cytoskeleton) respectively. Cell nuclei were identified using segmentation algorithms on the DAPI channel integrated in MetaMorph. Morphology was assessed by thresholding the Phalloidin signal per microwell. Differentiation was quantified by integrating the thresholded Nile Red signal per microwell. The measured parameters were extracted as indices averaged per total number of cells at day 11 (CellD11) in each respective microwell.

Immunohistochemistry

MSCs on arrays were fixed after 11 days in culture using 4% PFA (Fluka) for 15 min at RT. Adipogenic differentiation was detected by staining lipid content using Nile Red (Sigma, 1μg ml^{-1}). Nuclei were stained with DAPI (Sigma, 1μg ml^{-1}). After lipid vesicle imaging, cells on arrays were permeabilized for 5 min using 0.02% Triton-X prior to staining f-actin with Alexa488-phalloidin (Invitrogen, 2U ml^{-1}). Minimal staining volume for arrays is 1 ml to avoid drying-out.

Real-time quantitative RT-PCR

RNA extraction was performed using TRIzol Reagent (Ambion, life technologies) according to manufacturer's instruction. RNA was co-precipitated using 7.5μg RNase-free glycogen

(glycoblue, life technologies). cDNA was synthesized using 1µg RNA using iScript Select cDNA Synthesis Kit (Bio-Rad) and real-time PCR was carried out with the gene-specific primer sets (Supplementary Table S3) using Power SYBR Green PCR Master Mix (Applied Biosystems) with the Applied Biosystems 7900HT System. The expression of genes of interest was normalized to that of GAPDH in all samples. Fold changes were calculated with respect to the FNIII(9-10) control at the given stiffness. .

Microscopy and data analysis

All images were acquired with a Zeiss Axio Observer Z1 Inverted Microscope. An incubation chamber controlling temperature and CO2 levels allowed for live cell imaging. Image mosaics were acquired and reconstituted using MetaMorph software (MDS INC., USA). Full array scans in brightfield were taken at day 0 in order to determine initial cell numbers per well (CellD0). After 11 days of differentiation culture, arrays were stained with DAPI and the relevant metabolic/ IHC protocol. Scanning was performed field–wise in order to adjust focus variations using an automated custom 'scanslide' script. Contour plots where generated in R (R V3.1.2) by using the contour and kde2d functions of package graphics and MASS respectively. A multivariate analysis using generalized linear models (glm) or linear models (lm) was performed on the entire dataset to explain differentiation and proliferation (R V3.1.2). Initially, factors including randomization, protein combinations, substrate stiffness, replicates, initial cell density per microwell and all combinations thereof were considered to explain variation in adipogenic differentiation index (see also Supplementary Fig. S4). In a second step, the model was adjusted with the stepAIC procedure to minimize the inflation of variance. The final adjusted model, limited to relevant main factors and second-order interactions, accounted for more that a third of the measured variance (R^2 = 0.34). The significance of the different factors including substrate stiffness ($p < 0.001$), protein combinations ($p < 0.001$) and initial cell density ($p < 0.001$) was assessed with the drop1 procedure. The distribution of the residuals from the multivariate analysis was evaluated by the Tukey-Anscombe and the QQ-plots methods in order to verify that the assumptions of ANOVA (homoscedasticity, normality) were met. The produced averages were obtained by the LSMeans function of SAS software V9.0. All p values where adjusted with a Bonferroni correction to account for errors due to multiple comparisons.

Results and discussion

High-throughput screening of multifactorial microenvironments

Over the past decade a number of signaling pathways have been associated to the regulation of hMSC differentiation. Accordingly, Wnt and BMP signaling predominantly promote osteogenesis[14, 15] even though some reports challenged these findings by showing osteogenesis-inhibitory and pro-adipogenic effects.[16, 17] This suggests that protein actions could be highly context-dependent and possibly linked to other biochemical or biophysical signals. To better understand the multifactorial signaling system that controls hMSC

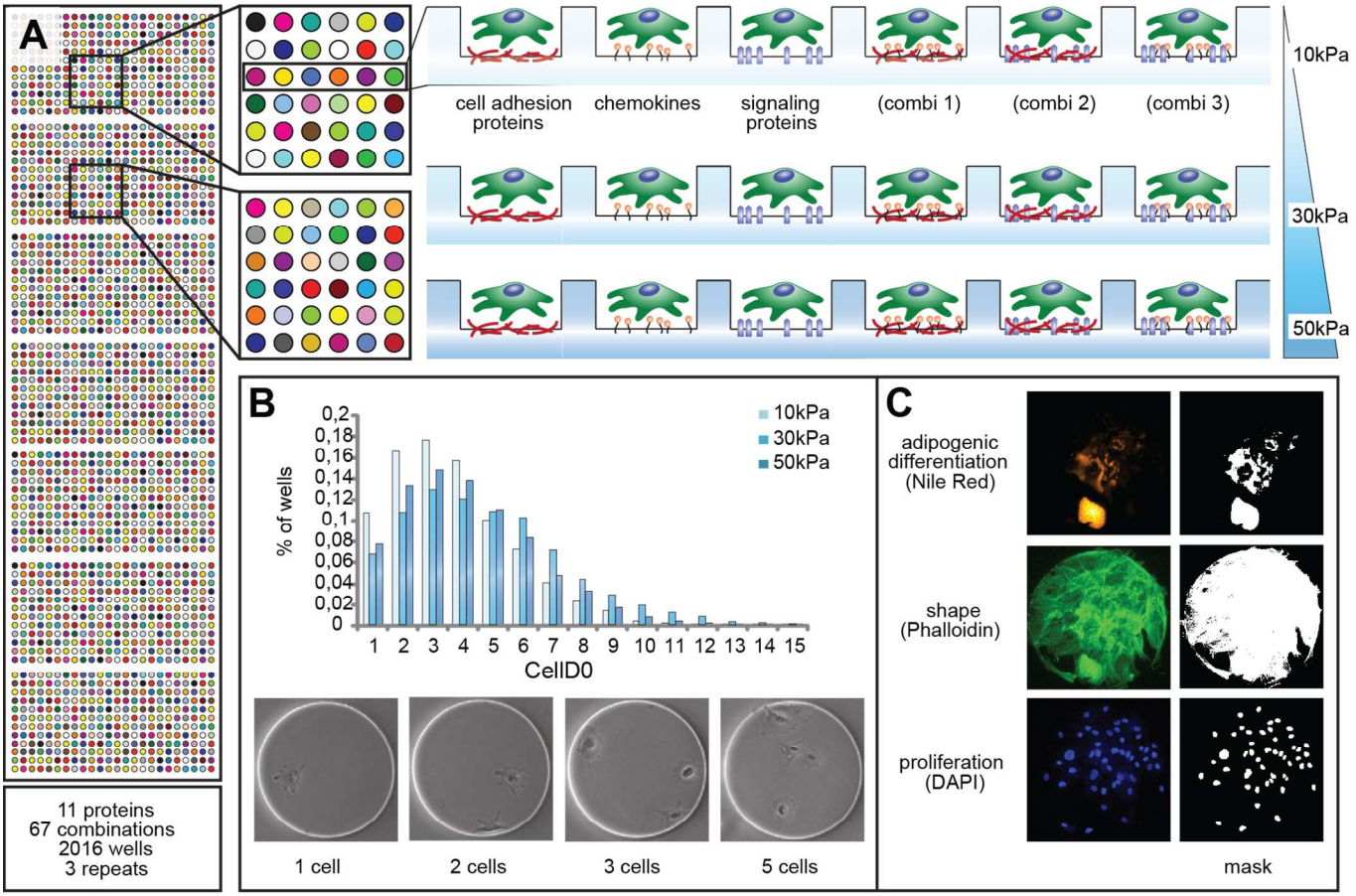

Fig. 1 Experimental design. (A) Schematic representation of the performed protein combinatorial assay on substrates of variable stiffness. (B) Seeded MSCs adhere in a similar fashion to all the microwell arrays regardless of the rigidity of the substrate. (C) Quantification of adipogenesis and cell surface area were performed by quantifying Nile Red and Phalloidin

differentiation, we interrogated the role of putative hMSC niche effectors by employing a previously developed artificial niche microarray technology.[13] We arrayed 67 combinations of 11 different proteins on hydrogel substrates with contrasted mechanical properties (Fig. 1 A). Nine proteins were chosen as agonist or antagonist of Wnt-, BMP- and Notch-signaling pathways as well as two cell-cell or cell-ECM interaction molecules (N-Cadherin and Laminin). We also employed a cell-binding fibronectin fragment 9 and 10 of the fibronectin type III module (FNIII(9-10)) in all the microenvironments to promote cell adhesion.

Each unique signaling microenvironment was printed 28 times per array. A fully randomized block design ensured that every microenvironment could be observed in at least eight distinct neighboring situations to avoid positional bias and local paracrine effects. The arrays were produced in triplicates allowing the collection of data in 84 microwells per protein combination and stiffness. Since the initial cell density per microwell can strongly influence adipogenic differentiation,[13] all niche arrays were imaged within four hours after seeding variable in the constructed statistical Generalized Linear Model (GLM). Notably, no initial difference in average cell density on arrays of variable matrix stiffness was observed (Fig. 1 B). After 11 days in adipogenic differentiation culture, cells were fixed and the extent of differentiation, measured by lipid accumulation stained by Nile Red, was quantified for every microwell (Fig. 1 C). A multivariate statistical analysis was performed on the complete dataset in order to document the relative importance (hierarchy) of each artificial niche and to quantify the contribution of the interactions between niche effectors to adipogenic differentiation (Supplementary Fig. S4).

We also quantified the hMSC surface area that was obtained by a cytoskeletal stain of fixed cells at the end of the experiment (Fig. 1 C). The rationale for including this read-out was to be able to correlate differentiation with modification of the cell surface area. Indeed, these two traits are strongly negatively correlated (R = -0.89) in all of the microenvironments we analyzed, as we show later on (Fig. 4 C). Higher lipid accumulation always resulted in smaller and increasingly round cells. In order to understand if this smaller

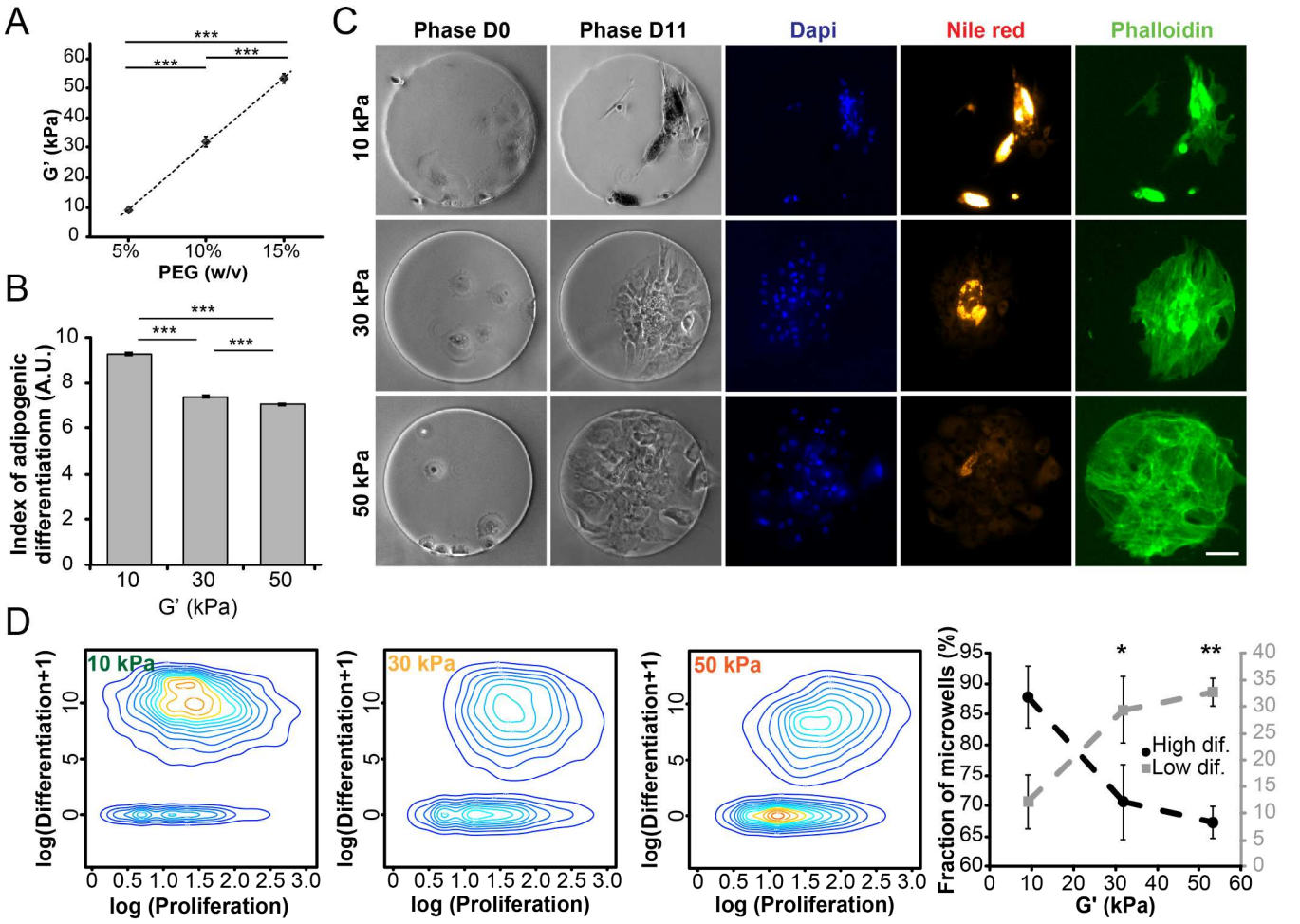

Fig. 2 MSCs cultured on artificial niche arrays with varying stiffness. (A) hMSCs were seeded on arrays of low (10kPa), intermediate (30 kPa) and high (50 kPa) elastic modulus, matching the mechanical properties of adipose tissue, muscle and cartilage. (B) Globally increasing stiffness of the substrate decreased adipogenic differentiation of hMSCs (C) as illustrated by Nile Red staining. (D) Scattering of all the observations as a function of proliferation and differentiation

and the initial cell densities were used as an explanatory surface area on soft gels was the result or was the cause of

higher adipogenic differentiation, we quantified cell surface area as early as six hours after seeding hMSCs, before the appearance of any lipid vesicle. We found that hMSC already acquired significantly lower ($p < 0.001$) cell surface areas on soft substrates (Supplementary Fig. S 5). This is in line with an extensive body of work demonstrating that stiffness-triggered cytoskeletal reorganization drives stem cell differentiation.[18]

Effect of substrate stiffness on adipogenic differentiation

In an attempt to recapitulate the range of mechanical properties to which hMSC can be exposed to *in vivo*[4], we produced arrays with shear moduli (G') ranging from 9 to 53kPa (corresponding to Young's moduli E of ca. 30-150kPa). This stiffness range was achieved by adapting the concentration of PEG precursors during hydrogel formation as previously reported[13] (Fig. 2 A). Current patterning methods limit the reproducibility of arrays below this indicated stiffness range. Nonetheless, in this study, the lowest probed stiffness reflects near physiological regimes, as adipose tissues, depending on their relative location *in vivo*, have been shown to display ranges of elastic moduli up to 30kPa.[19-21] As expected, the increase in matrix stiffness resulted in a decreased average adipogenic differentiation (Fig. 2 B-C). Of note, when the observations made in every microwell were plotted as a function of differentiation and proliferation, hMSCs responses segregated into two distinct populations; one population characterized by quantifiable lipid accumulation and another where differentiation remained under or very close to the detection threshold. The relative importance of each population was significantly dependent on the rigidity of the culture substrate ($p < 0.001$) (Fig. 2 D). Increasing stiffness clearly prevented a larger fraction of hMSCs to reach detectable lipid vesicle accumulation.

These data confirm that the lineage specification of stem cells can be determined by matrix elasticity.[4, 22, 23] Intriguingly, the observation of adipogenesis on artificial niches also revealed that lower stiffness allows a larger population of MSC to accumulate fat rather than a higher lipid content per differentiated cell. This challenges how the heterogeneous behavior of MSC is explained by imperfect isolation[24], as our data indicates that heterogeneity in hMSC fate can be at least partially driven by environmental cues (Fig. 2 D).

Elasticity modulates the responsiveness to commitment cues

Our high-throughput artificial niche screening approach offers the unique ability to observe, in a single experiment, the combined effects of biophysical and biochemical cues. This

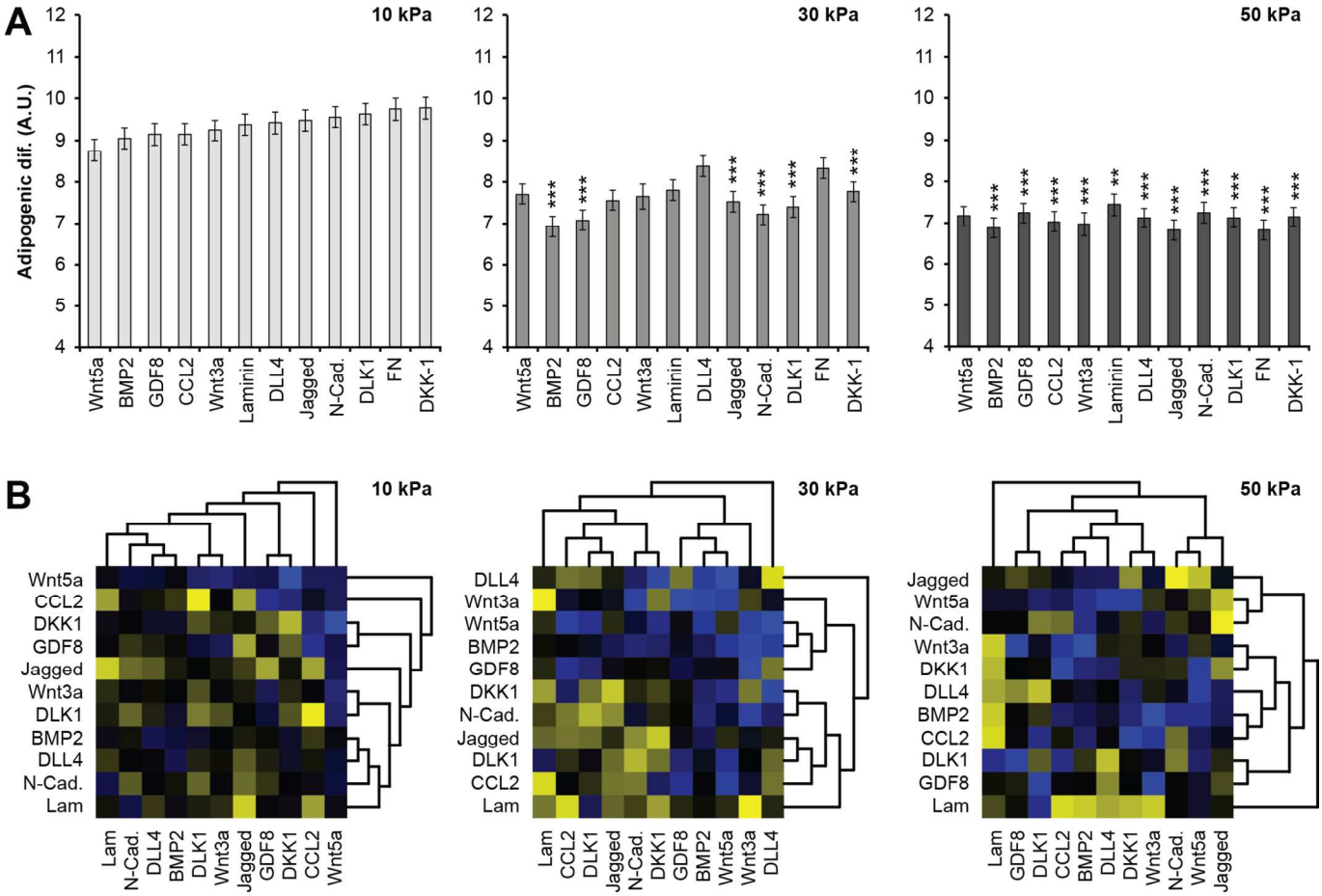

Fig. 3 Effects of spotted proteins on adipogenic differentiation of hMSC across soft, intermediate and hard substrates. (A) Considering single proteins alone, the effect of stiffness was clearly larger than the effect of any protein. However within each stiffness class, the biochemical microenvironment remained explicative of adipogenic differentiation. (B) Hierarchical clustering illustrating the interactions between proteins, across different stiffnesses was performed to discriminate between context-dependent and dominant proteins. The eleven proteins could be classified as having dominating or context-dependent effects. Yellow and blue colors correspond to high and low levels of adipogenic

sheds light on synergistic combinations highly instructive of stem cell fate. We first looked at the effect of the spotted protein across three levels of stiffness. We found that proteins could never counteract the effect of matrix elasticity on adipogenesis (Fig. 3 A). Each stiffness imposed a strictly non-overlapping range of differentiation (Fig. 4 C). However, for a given stiffness a significant protein-dependent effect on adipogenesis can be observed. These observations suggest that matrix stiffness is the key factor determining the range of achievable adipogenic differentiation. Within stiffness-imposed windows, biochemical cues seem to fine-tune adipogenic differentiation. Moreover, we observed that the effect of proteins can be highly context-dependent. For instance Jagged1, CCL2 or Wnt5a clearly showed a smaller decrease in differentiation upon stiffness increase compared to the prediction of a linear model (Supplementary Fig. S 6).
This context-dependent effect results in a ranking of the proteins effects that is only poorly preserved across the three stiffness ranges, as shown by a Kendall's tau rank correlation coefficient varying between 0.2 and 0.5 and the hierarchical

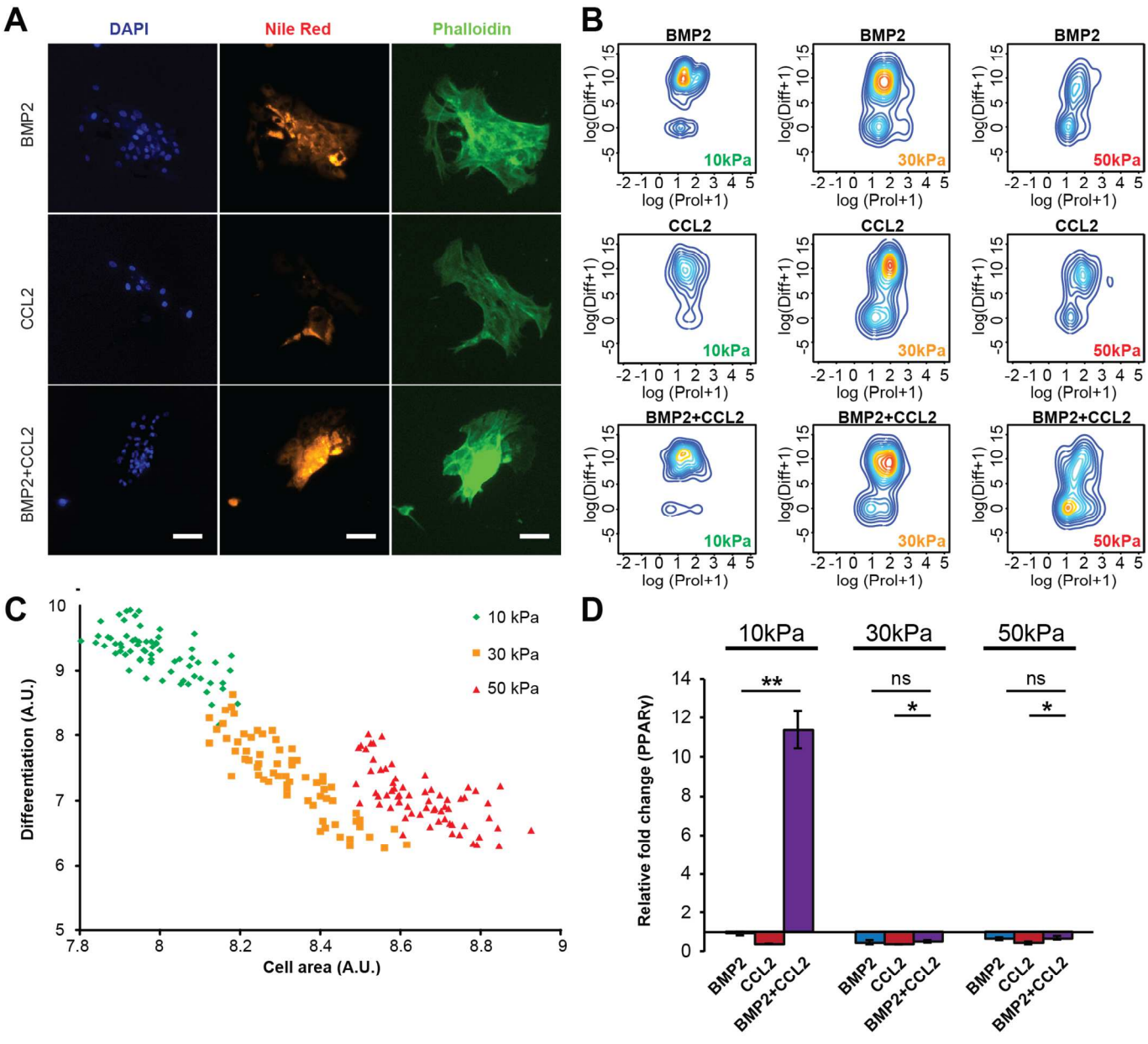

Fig. 4 The combination of BMP2 and CCL2 induces strong adipogenic differentiation (A) When cultured in microwells containing either BMP2 or CCL2, hMSCs showed reduced levels of adipogenic differentiation, whereas the combination of the two proteins strongly increased lipid vesicle accumulation. (B) At the population level, the negative effect of CCL2 is explained by an average low but consistent accumulation of lipid vesicle. On the contrary, BMP2 was found to decrease the frequency of detectable lipid accumulation. The combination of the two proteins allowed higher quantity and a higher frequency of lipid accumulation. (D) This interaction was found to be occurring only for an elastic modulus approaching the elastic modulus of native adipose tissue (here G'=10kPa) and was confirmed by quantitative analysis of gene expression,

clustering of the different combinations (Fig. 3 B). Together, these results demonstrate that the interaction between physical and biochemical cues is dominated by the physical cue and that proteins largely differ in the ability to maintain a consistent effect across different stiffnesses.

Effect of tethered proteins on adipogenic differentiation

Although less dominant than substrate stiffness, some of the 67 tethered protein microenvironments were found to efficiently contribute to adipogenesis.. Documenting the effect of each protein or protein combination confirmed the negative effect of BMP2 on adipogenic differentiation on all levels of stiffness (Fig. 3 A). We also observed that Wnt signaling impaired adipogenic differentiation in our experimental setup. Conversely, the repression of the Wnt pathway by spotting an antagonist (DKK1) favored adipogenesis. Furthermore, triggering Notch signaling (Jagged, DLL4) or antagonizing it (DLK1) had effects that are dependent on the stiffness of the substrate. Cell-cell or cell-matrix interaction proteins, such as Laminin, Jagged or N-cadherin, and Notch signals showed additive pro-adipogenic effects. Whether these proteins are acting by imposing cytoskeleton remodeling[25, 26] or directly on the lipid metabolism needs to be further elucidated.

When all single proteins were combined, hierarchical clustering showed that every protein had either context-dependent or more dominant effects (Fig. 3 B). On soft hydrogels, Wnt5a had a dominant effect as it imposed lower adipogenic differentiation and larger cell area when spotted in combination with any of the other 10 proteins. Similarly, Laminin, Jagged1 and N-cadherin had a rather dominant effect, promoting higher differentiation and smaller cell areas. In contrast, proteins such as CCL2 or DLK1 were found in both pro- and anti-adipogenic microenvironments. We also observed that the classification as dominant or context-dependent effectors was strongly altered upon increase of the substrate stiffness. The level of organization in the three stiffness clusters is decreasing with increasing stiffness. Proteins such as BMP2, Wnt5a, Jagged or Laminin 1 are having less and less dominant effect on cell area and on differentiation when rigidity of the substrate increased.

The effect of other proteins such as CCL2, DKK or DLK1 remained context-dependent across the investigated stiffness range. When all the combinations were taken into account, the negative correlation of substrate stiffness and adipogenesis was maintained for all protein combinations (Fig. 3 B). We demonstrate how the mechanical stimulus can synergistically enhance or repress a given biochemical cue. We rule out that the immobilized proteins themselves can serve as mechanical triggers through differential anchoring on varying stiffness[27], as in all conditions the adhesion on the PEG microwell arrays was mediated by a short fragment of fibronectin. Furthermore, through our designed immobilization scheme of proteins via (i) Michael-type addition and (ii) incorporated Protein A, the amount of reaction sites was held constant and a possible conformation change of proteins consequently unlikely as additionally demonstrated previously by homogeneous immunohistochemical staining of immobilized proteins on varying stiffness[13].

Artificial niche screening reveals synergistic interactions

The artificial niche platform was finally used to investigate synergistic effects arising from 3-way combinations (two proteins across three stiffness domains). Here our approach offers the unique opportunity to contextualize the synergistic interaction and to classify them as stiffness-dependent or stiffness-independent. For instance, we observed that on average both BMP2 and CLL2 lowered adipogenesis when spotted alone on the softest substrates (Fig. 4 A-B). It appeared that the negative effect of CCL2 was due to an average lower Nile red signal in all microwells containing only this protein, although the frequency of detectable differentiation was very high in the CCL2 microwells. BMP2 had the exact opposite effect, promoting high accumulation of lipid only at a low frequency. Interestingly, when these two proteins were spotted in combination, a microenvironment supporting strong adipogenesis was created. This microenvironment triggered higher lipid accumulation at higher frequency, demonstrating the synergy of the two modes of action. Noticeably, this interaction did not resist the increase of stiffness probably because the negative effect of BMP2 became dominant (Fig. 4 B and D). These observations were confirmed by the analysis of relative gene expression using real-time qPCR of key adipogenic genes, such as PPARγ (Fig. 4 C) and lipoprotein lipase (LPL), C/EBPα and adiponectin (AdipoQ) (Supplementary Fig. S 7).

Conclusions

We demonstrate in this study that the elasticity of a given substrate can modulate the responsiveness of mesenchymal stem cells to differentiation signals. The high-throughput modulation of micro-environmental parameters in a single experiment allowed the establishment of a hierarchy of extrinsic cell fate effectors, where mechanical stimuli of adipogenic differentiation override the biochemical one. Moreover, dissecting the determinants of adipogenesis in a systematic fashion shed light on how this process is coordinated at the level of the cell population. We could demonstrate that two concurrent modes-of-action are at play. First, we found that the frequency of positive cells for lipid accumulation was mostly determined by substrate stiffness. But we also demonstrated that the extent of lipid accumulation was preferentially driven by the biochemical context. The intricate action of these two mechanisms was illustrated for example by the synergistic interaction between CCL2 and BMP2, yielding a highly potent microenvironment capable of increasing both frequency and intensity of adipogenesis specifically on low stiffness substrates. Taken together, the presented work emphasizes the need of performing experiments targeted to identify niche signals in a relevant biophysical context.

Acknowledgements

We thank Alessandra Griffa for support with image analysis. The fibronectin fragment used in this study was generously provided by Mikael Martino and Jeffrey Hubbell (EPFL, Switzerland). We thank Martin Ehrbar from the University of Zurich for providing recombinant BMP-2. This study was funded by the Swiss National Science Foundation grant CR23I3_143766 and the EU FP7 grant 'BIODESIGN' FP7-NMP-2010-LARGE-4.

Notes and references

[a] Laboratory of Stem Cell Bioengineering (LSCB), Institute of Bioengineering (IBI), Ecole Polytechnique Fédérale de Lausanne (EPFL), Lausanne, Switzerland

[b] Institute of Chemical Sciences and Engineering, École Polytechnique Fédérale de Lausanne (EPFL), Lausanne CH-1015, Switzerland
¶ S.H. and S.G. contributed equally to this work
* To whom correspondence should be addressed: matthias.lutolf@epfl.ch

† Electronic Supplementary Information (ESI) available: [details of any supplementary information available should be included here]. See DOI: 10.1039/b000000x/

1 D. E. Discher, D. J. Mooney and P. W. Zandstra, Science, 2009, 324, 1673-1677.
2 H. V. Unadkat, M. Hulsman, K. Cornelissen, B. J. Papenburg, R. K. Truckenmuller, A. E. Carpenter, M. Wessling, G. F. Post, M. Uetz, M. J. Reinders, D. Stamatialis, C. A. van Blitterswijk and J. de Boer, Proceedings of the National Academy of Sciences of the United States of America, 2011, 108, 16565-16570.
3 F. Guilak, D. M. Cohen, B. T. Estes, J. M. Gimble, W. Liedtke and C. S. Chen, Cell Stem Cell, 2009, 5, 17-26.
4 A. J. Engler, S. Sen, H. L. Sweeney and D. E. Discher, Cell, 2006, 126, 677-689.
5 J. R. Tse and A. J. Engler, Plos One, 2011, 6, e15978.
6 P. M. Gilbert, K. L. Havenstrite, K. E. Magnusson, A. Sacco, N. A. Leonardi, P. Kraft, N. K. Nguyen, S. Thrun, M. P. Lutolf and H. M. Blau, Science, 2010, 329, 1078-1081.
7 L. MacQueen, Y. Sun and C. A. Simmons, Journal of the Royal Society, Interface / the Royal Society, 2013, 10, 20130179.
8 M. P. Lutolf and J. A. Hubbell, Nature biotechnology, 2005, 23, 47-55.
9 C. J. Flaim, D. Teng, S. Chien and S. N. Bhatia, Stem cells and development, 2008, 17, 29-39.
10 Y. Soen, A. Mori, T. D. Palmer and P. O. Brown, Molecular systems biology, 2006, 2, 37.
11 R. Derda, L. Li, B. P. Orner, R. L. Lewis, J. A. Thomson and L. L. Kiessling, ACS chemical biology, 2007, 2, 347-355.
12 M. A. LaBarge, C. M. Nelson, R. Villadsen, A. Fridriksdottir, J. R. Ruth, M. R. Stampfer, O. W. Petersen and M. J. Bissell, Integr Biol (Camb), 2009, 1, 70-79.
13 S. Gobaa, S. Hoehnel, M. Roccio, A. Negro, S. Kobel and M. P. Lutolf, Nat Methods, 2011, 8, 949-955.
14 F. Gori, T. Thomas, K. C. Hicok, T. C. Spelsberg and B. L. Riggs, Journal of bone and mineral research : the official journal of the American Society for Bone and Mineral Research, 1999, 14, 1522-1535.
15 T. F. Day, X. Guo, L. Garrett-Beal and Y. Yang, Dev Cell, 2005, 8, 739-750.
16 G. M. Boland, G. Perkins, D. J. Hall and R. S. Tuan, J Cell Biochem, 2004, 93, 1210-1230.
17 H. Huang, T. J. Song, X. Li, L. Hu, Q. He, M. Liu, M. D. Lane and Q. Q. Tang, Proceedings of the National Academy of Sciences of the United States of America, 2009, 106, 12670-12675.
18 Y. Sun, C. S. Chen and J. Fu, Annual review of biophysics, 2012, 41, 519-542.
19 T. A. Krouskop, T. M. Wheeler, F. Kallel, B. S. Garra and T. Hall, Ultrasonic imaging, 1998, 20, 260-274.
20 M. Geerligs, G. W. Peters, P. A. Ackermans, C. W. Oomens and F. P. Baaijens, Biorheology, 2008, 45, 677-688.
21 N. Alkhouli, J. Mansfield, E. Green, J. Bell, B. Knight, N. Liversedge, J. C. Tham, R. Welbourn, A. C. Shore, K. Kos and C. P. Winlove, Am J Physiol-Endoc M, 2013, 305, E1427-E1435.
22 N. D. Evans, C. Minelli, E. Gentleman, V. LaPointe, S. N. Patankar, M. Kallivretaki, X. Chen, C. J. Roberts and M. M. Stevens, European cells & materials, 2009, 18, 1-13; discussion 13-14.
23 F. M. Watt, P. W. Jordan and C. H. O'Neill, Proceedings of the National Academy of Sciences of the United States of America, 1988, 85, 5576-5580.
24 A. Alhadlaq and J. J. Mao, Stem cells and development, 2004, 13, 436-448.
25 B. D'Souza, A. Miyamoto and G. Weinmaster, Oncogene, 2008, 27, 5148-5167.
26 E. Giniger, Curr Opin Genet Dev, 2012, 22, 339-346.
27 B. Trappmann, J. E. Gautrot, J. T. Connelly, D. G. Strange, Y. Li, M. L. Oyen, M. A. Cohen Stuart, H. Boehm, B. Li, V. Vogel, J. P. Spatz, F. M. Watt and W. T. Huck, Nature materials, 2012, 11, 642-649.